ISSN 2075-1133, Inorganic Materials: Applied Research, 2018, Vol. 9, No. 1, pp. 57–65. © Pleiades Publishing, Ltd., 2018.
Original Russian Text © A.I. Epishin, B.S. Bokstein, I.L. Svetlov, B. Fedelich, T. Feldmann, Y. Le Bouar, A. Ruffini, A. Finel, B. Viguier, D. Poquillon, 2017, published in Materialovedenie, 2017, No. 5, pp. 3–12.

A Vacancy Model of Pore Annihilation During Hot Isostatic Pressing of Single Crystals of Nickel-Base Superalloys

A. I. Epishin[a], *, B. S. Bokstein[b], I. L. Svetlov[c], B. Fedelich[d], T. Feldmann[d], Y. Le Bouar[e], A. Ruffini[e], A. Finel[e], B. Viguier[f], and D. Poquillon[f]

[a] *Technical University of Berlin, Berlin, Germany*
[b] *National Technological University MISiS, Moscow, Russia*
[c] *All-Russian Scientific Research Institute of Aviation Materials, Moscow, Russia*
[d] *Federal Institute for Materials Research and Testing, Berlin, Germany*
[e] *Laboratory of Microstructure Studies and Mechanics of Materials, CNRS/ONEPA, Châtillon, France*
[f] *University of Toulouse, Toulouse, France*
** e-mail: Alex_epishin@yahoo.de*

Received October 19, 2016

Abstract—An improved diffusion model of pore annihilation during hot isostatic pressing of single crystals of nickel-base superalloys is proposed. The model considers dissolution of pores by emission of vacancies and their diffusion sink to low-angle boundaries. The calculation, which takes into account pore size distribution, predicts the kinetics of pore annihilation similar to experimental one.

Keywords: single crystals of nickel-base superalloys, hot isostatic pressing (HIP), porosity, diffusion, vacancies
DOI: 10.1134/S2075113318010100

INTRODUCTION

The blades of the hot part of gas-turbine engines operate under extremely severe conditions, which include various types of thermomechanical loads and corrosion effect at temperatures of up to 1100–1150°C. Turbine blades are cast from heat-resistant and corrosion-resistant nickel-base superalloys with single-crystal structure, where there are no high-angle boundaries, where oxidation and intergranular failure occur. During directional solidification of blades via dendritic growth, solidification (*S*) pores with sizes up to several tens of microns are formed in the interdendritic region, while during further high-temperature homogenization and dissolution of nonequilibrium eutectics smaller homogenization (*H*) pores with the size of 5–10 μm are formed [1–3]. The volume fraction and pore size are determined both by the chemical composition of alloy [4] as well as by the conditions of crystallization and heat treatment [5, 6]. The porosity in single-crystal superalloys is small and does not exceed several tenths of a percent by volume. However, it significantly reduces the fatigue strength of single-crystal superalloys in the temperature range of 20–750°C [7]; therefore, single-crystal blades are exposed to hot isostatic pressing (HIP). In spite of the industrial application of HIP, the physical mechanism of pore healing in single-crystal superalloys during the production of blades is not quite clear, which complicates the choice of technological parameters of HIP (temperature T, pressure p, and duration t), as well as the prediction of the lifetime of HIP-treated blades. There is experimental evidence that during HIP pores annihilate according to two mechanisms: vacancy dissolution (vacancy mechanism) [8, 9] and dislocation creep (dislocation mechanism) [7, 10]. The formation of a continuous γ' phase around a pore and in the place of its annihilation [9, 11] as a result of inflow of rapidly diffusing aluminum atoms to the pore surface supports the vacancy mechanism. The observation of dislocation loops creeping along octahedral planes near a pore using transmission electron microscope (TEM) [7, 10] supports the dislocation mechanism. It is evident that both mechanisms may act simultaneously; however, their relative activity depends on parameters of HIP, namely, temperature T and pressure p. Therefore, in order to describe the kinetics of HIP in a broad range of technological parameters, it is necessary to develop the models of pore annihilation considering both mechanisms.

The vacancy mechanism of pore annihilation was initially suggested for the description of sintering powder materials [12–14]. Various models of materials with pores were considered: central pore in the grain bulk, the pore shifted from the grain center, and the pore at the grain boundary [14]. In this case, it was usually assumed that the main driving force of the contraction of pores results from their surface tension.

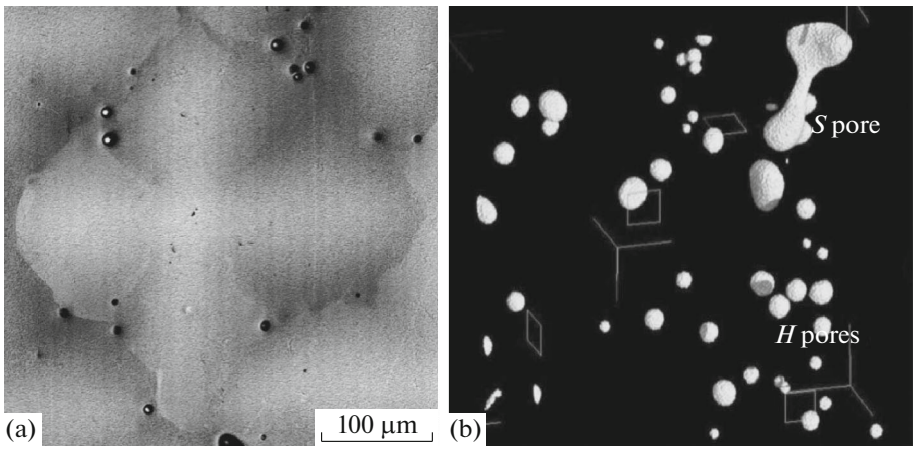

Fig. 1. Pores in heat-treated single crystal of nickel-base superalloy CMSX-4: (a) cross section of dendrite with (001) plane, contrast in backscattered electrons (BSE); (b) synchrotron X-ray tomogram of porosity, volume is 295 × 180 × 210 μm^2 [2].

It was proposed later that annihilation of pores during HIP of single-crystal superalloys may also occur via the vacancy mechanism [8, 9]. In the proposed model of vacancy dissolution of pores, the effect of the external applied pressure was considered in addition to surface tension. In this work, an improved vacancy model taking into account pore size distribution, which was shown significantly influences on the kinetics of pore annihilation, is proposed. Therefore, this distribution of pore size should be considered in the choice of the duration of HIP.

PHYSICAL MODEL OF DIFFUSION MECHANISM

Micropores in superalloy single crystals are formed in the interdendritic region at the final stage of solidification (*S* pores) or during the dissolution of nonequilibrium inclusions of eutectic γ′-phase during high-temperature homogenization (*H* pores). In Fig. 1a, SEM (scanning electron microscope) images of porosity in a heat-treated single crystal of CMSX-4 alloy are given, while in Fig. 1b a synchrotron X-ray tomogram of porosity in this single crystal is given. In Fig. 1b, numerous spherical pores, *H* pores, and the dumbbell-shaped *S* pore can be observed.

It can be assumed that the pores in superalloy single crystals are not filled with gas. This assumption is based on: vacuum melting of superalloy single crystals, high purity of the employed batch (content of O_2 and N_2 gases is at 1–2 ppm), and low solubility of O_2 and N_2 in nickel [15, 16]. In addition, there are no oxides and nitrides on the pore surface, which could be formed during high-temperature treatment upon pore filling with oxygen or nitrogen.

Owing to surface tension, the equilibrium concentration of vacancies at the surface of vacuum pores c_p exceeds that in the bulk single crystal c^0:

$$c_p = c^0 \exp\left(\frac{2\gamma_p V_a}{R_p k T}\right) \approx c^0\left(1 + \frac{2\gamma_p V_a}{R_p k T}\right), \quad (1)$$

where γ_p is the specific surface energy, R_p is the pore radius, V_a is the atomic volume, k is the Boltzmann constant, and T is the absolute temperature. The negative radial gradient of the concentration of vacancies ∇c near the pore surface causes their diffusion sink, which initiates additional emission of vacancies by the pore surface and its vacancy dissolution. However, as will be shown below, this process in superalloy single crystals is active only at very small pore sizes (on the order of several tens of nanometers); therefore, in the evaluation of the total duration of HIP of single crystals with pores with sizes of several tens of microns, diffusion contraction of pore under the action of surface tension can be neglected.

When external hydrostatic pressure p is applied to the single crystal, an equilibrium concentration of vacancies is preserved in the bulk single crystal and near the free pore surface. However, it decreases at the external loaded surface of single crystal, as well as near defects of the crystal structure, such as low-angle boundaries (LABs) and edge dislocations, because during the annihilation of a vacancy at the external surface, LABs, or edge dislocation the volume of single crystal decreases by V_a and, consequently, the external pressure performs mechanical work pV_a. The equilibrium concentrations of vacancies at the external surface and near the edge dislocation core are equal to:

$$c_e = c^0 \exp\left(-\frac{pV_a}{kT}\right) \approx c^0\left(1 - \frac{pV_a}{kT}\right). \quad (2)$$

The negative gradient of the concentration of vacancies ∇c from pore to the external surface initiates the diffusion of vacancies in this direction and, consequently, dissolution of pore. However, this process proceeds fairly quickly only in the case of near-surface

pores and very slowly in the case of pores in the depth of a single crystal owing to the large diffusion path of vacancies x. It is known that the time of diffusion is proportional to the square of the diffusion path, $t \sim x^2$.

According to Coble [12], pore annihilation during sintering of powder material may occur by the diffusion of vacancies from pores to edge grain-boundary dislocations, causing their climb (reduction of half extraplanes) in the plane of grain boundary. Almost all dislocations in the undeformed superalloy single crystals are integrated in LABs; therefore, LABs can represent an alternative vacancy sink to the external surface. However, the following question arises in this case: Are the bulk density of LABs in single-crystal superalloy and their sink strength (the parameter characterizing the ability of grain boundaries to annihilate vacancies) sufficient for effective absorption of vacancies during HIP? This question can be qualitatively answered in the following way. Sinks and sources of vacancies are the same objects which absorb or emit vacancies depending on the existing thermodynamic conditions. As follows from the diffusion mechanism of H pore formation at high-temperature homogenization [3], the number of sources of vacancies in superalloy single crystals is sufficient for the growth of H porosity. Therefore, it can be anticipated that they (already sinks) are sufficient for pore annihilation during HIP, because the volume fraction of all $S + H$ pores is comparable to the volume fraction of H pores.

According to [17], the sink power of grain boundaries is determined by several factors, among which the most important is the density of grain-boundary dislocations, that is, the distance between dislocations in the boundary plane. The sink power of grain boundaries was considered in detail during the study of annihilation of vacancies formed during radiation exposure. It was shown in [18, 19] that the sink power of grain boundaries increases with the density of grain-boundary dislocations, that is, the misorientation of neighboring grains. However, it achieves saturation at misorientation of about 3° owing to the superposition of stress fields of individual grain-boundary dislocations. Therefore, grain boundaries with misorientation higher than 3° should be regarded as perfect planar sinks. In Fig. 2, the calculated plot of normalized sink power of LABs in aluminum vs. misorientation is given [18]. Similar dependences were obtained in [19] in the case of LABs in copper.

Single-crystal castings of superalloys possess defective dendritic-cellular structure, which is formed during directional solidification. As most materials, dendritic-cellular superalloy single crystals possess subgrain structure (Fig. 3a). Each dendrite can be regarded as an individual columnar subgrain. According to X-ray analysis [20], the crystallographic misorientation between neighboring dendrites may amount to several degrees (Fig. 3b). Dendritic arms of second and third orders also possess a slightly different orientation as follows from the orientational FSE (forescattered electrons) contrast in Fig. 3a. There are subgrains of another level (mosaic blocks) inside dendritic arms with a significantly smaller misorientation up to 0.1°. These boundaries are not seen in the FSE image; however, they can be visualized by microetching. The structure of low-angle boundaries can be observed in the TEM image of the structure of superalloy in Fig. 4. It is clear that low-angle boundaries represent networks of dislocations, which corresponds to the conventional model of LAB. It is known that the walls of edge dislocations form tilt LABs, while the networks of screw dislocations form twist SABs; in this case, the grain-boundary misorientation angle is determined by the density of the dislocation network. For example, the distance between dislocations in the case of LABs in superalloy between neighboring dendrites or dendritic arms with the misorientation of 1° is ≈15 nm, while in the case of intradendritic LAB with the misorientation of less than 0.1°, the dislocation distance is larger than 150 nm.

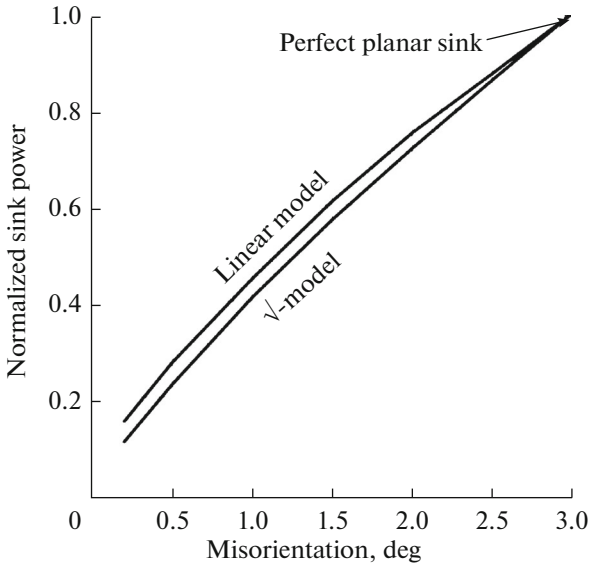

Fig. 2. Calculated sink power of low-angle boundary in FCC of aluminum at the subgrain radius of 100 nm and temperature of 300°C [18].

In Fig. 5, a typical spherical H pore in the single crystal of CMSX-4 alloy after 0.5 h of HIP at 1288°C/103 MPa is given. It is clear that a continuous shell of the γ′ phase formed around the pore, which can be considered as evidence for diffusion inflow of fast aluminum atoms to the pore, which compensates the counterflow of vacancies emitted by the pore surface. Ringlike facets representing the intersection lines of the spherical pore surface with crystallographic planes {012} can be seen on the pore surface. The same {012} faceting of the pore surface was previously observed by the authors in [22, 23] after annealing at 1250°C in diffusion couples of superalloy CMSX-10/Ni.

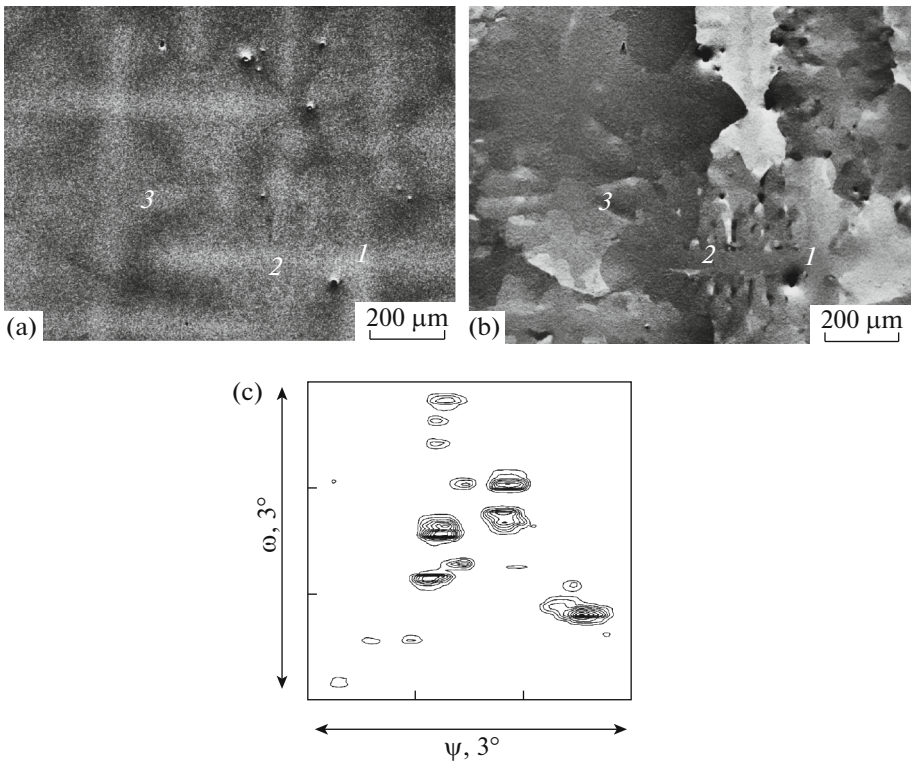

Fig. 3. The subgrain structure of the single crystal of CMSX-4 alloy at cross section (001): (a) BSE contrast by mean atomic number, (b) orientation contrast FSE (numerals *1*, *2*, and *3* correspond to dendritic arm of first, second, and third orders, respectively), and (c) X-ray orientation scan with area about 1 mm^2 [21].

Because in the latter case the pore growth occurs via the Kirkendall diffusion mechanism, it is reasonable to assume that the mechanism for the formation of {012} facets during HIP is also diffusion; i.e., the condensation or emission of vacancies by the pore is accompanied by specific {012} faceting of the pore surface.

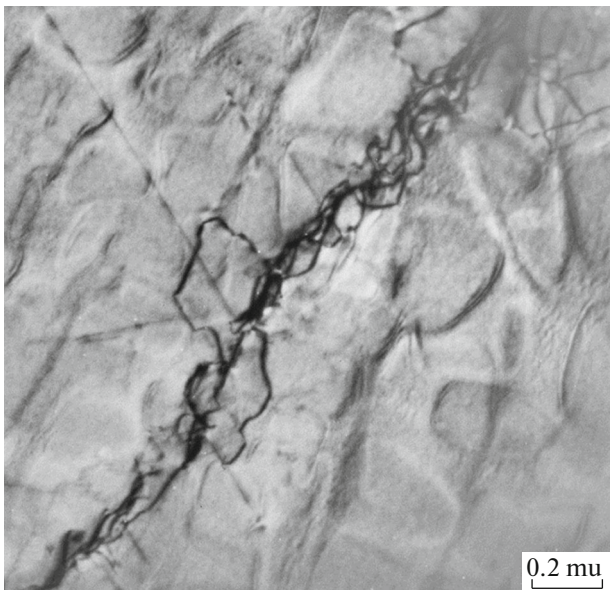

Fig. 4. Dislocation structure of LAB in the single crystal of CMSX-4 alloy after creeping at 1288°C/10 MPa, TEM.

It should be noted that all pores in superalloy single crystals are located on LABs (Fig. 1a); therefore, we could anticipate a more intense diffusion of vacancies and atoms along the LAB. However, as follows from Fig. 5, the thickness of the γ′ shell around the pore is constant, which implies that the diffusion flow at the pore surface does not depend on direction. At these high homologous temperatures $T_{hom} \approx 0.97$[1], the bulk diffusion in crystal lattice is so rapid [23] that the diffusion along LAB with the low dislocation density does not have a significant importance. It is also notable that *H* pores possess a clear spherical shape after high-temperature homogenization (before HIP) and after HIP.

It is known that, in the case of equilibrium pore on the subgrain boundary, the following relation should be fulfilled: $\cos\theta = \gamma_s/2\gamma_p$, where θ is the angle formed by the pore surface with LAB and γ_s and γ_p are the specific surface energies of subgrain boundary and pore surface, respectively. In the case of spherical pores, $\theta \approx 90°$ and, consequently, $\gamma_s \ll \gamma_p$. In nickel and nickel-base superalloys, the surface energy is ~2 J m^{-2} [24–

[1] $T_{hom} = T_{HIP}/T_S$, where T_{HIP} = 1561 K and T_S = 1612 K are the temperature of HIP and the solidus of CMSX-4 alloy, respectively.

28]; therefore, $\gamma_s \ll 2$ J m^{-2}. This value is in agreement with the results of experimental and theoretical study of the grain-boundary energy of FCC metals [17, 29]. According to [29], the energy of LAB with misorientation of less than 5° in nickel is less than several tenths of J m^{-2}. The independence of diffusion flow at the pore surface on the direction and low value of γ_s are a sufficient reason to neglect the boundary location of pores and consider only the bulk diffusion of vacancies.

Assuming LAB as the main vacancy sink during HIP, we can propose the physical model of the vacancy dissolution of pores given in Fig. 6. In order to simplify further consideration, let us assume in analogy with [14, 29] that the pore is located in the center of subgrain and the subgrain is bordered by LAB, which is formed by the networks of edge dislocations. The pore emits vacancies, which diffuse to LAB and annihilate on edge dislocations contracting their half extraplanes as shown by arc arrow. As a result of the emission of vacancies, the pore size decreases, while the subgrain size decreases as a result of the contraction of half extraplanes of dislocations. It is convenient to consider the pore and subgrain as concentric spheres with the radii of R_p and R_s, respectively (the indices p and s refer to pore and subgrain, respectively), to describe the diffusion of vacancies mathematically in this physical model (Fig. 6). The R_s-to-R_p ratio can be evaluated from the volume fraction of pores in the single crystal f_p. In heat-treated single crystals of CMSX-4 alloy, $f_p \approx 0.22\%$ [7, 10]; therefore, $R_s/R_p = f_p^{1/3} \approx 7.7$.

Assuming that the mean pore size in these single crystals $\overline{R}_p \approx 4.35$ μm [2], we get $\overline{R}_s \approx 7.7\overline{R}_p \approx 33.5$ μm, which is close to the radius of the cross section of dendritic arms. Thus, this model of subgrain can be considered as the subgrain of dendritic origin, i.e., the grain formed during the growth of dendritic arms.

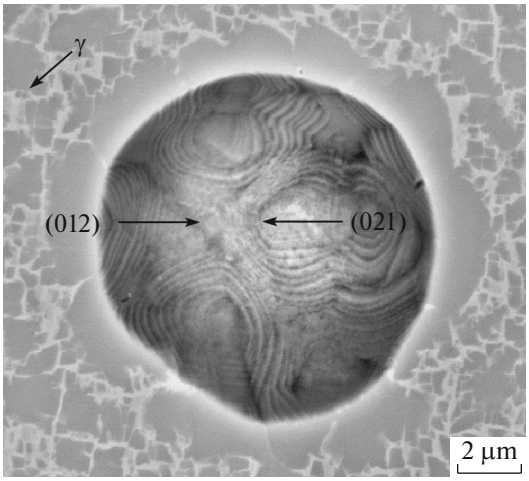

Fig. 5. Pore faceted with {012} planes in the single crystal of CMSX-4 alloy after 0.5 h of HIP at 1288°C/103 MPa. There is a γ′ shell around the pore. Section (012), SEM, BSE.

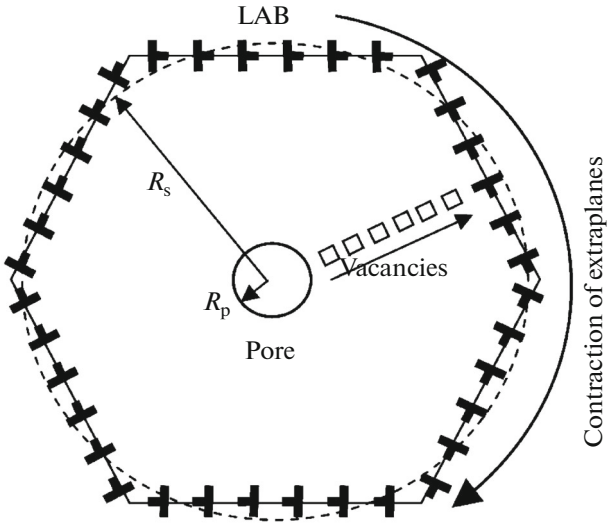

Fig. 6. The model of vacancy dissolution of pores during HIP: the central pore in a subgrain bordered by LABs consisting of edge dislocations.

SOLUTION OF DIFFUSION PROBLEM

The radial distribution of the concentration of vacancies c in the model in Fig. 6 can be evaluated under the assumption that the diffusion process is stationary; i.e., the concentrations of vacancies at each point remain constant:

$$\frac{\partial c(r,t)}{\partial t} = 0, \tag{3}$$

where r is the distance from the center of pore and t is time.

In this case, according to Fick's second law,

$$D_V \Delta c(r) = \frac{\partial c(r)}{\partial t} = 0, \tag{4}$$

where D_V is the diffusion coefficient of vacancies. In spherical coordinates, Eq. (4) takes form

$$\Delta c(r) = \frac{1}{r^2}\frac{\partial}{\partial r}\left[r^2 \frac{\partial c(r)}{\partial r}\right] = 0. \tag{5}$$

Its solution is

$$c(r) = \frac{A}{r} + B, \tag{6}$$

where A and B are constants determined by the boundary conditions:

$$c_p = c(R_p), \tag{7}$$

$$c_s = c(R_s), \tag{8}$$

where c_p and c_s are the concentrations of vacancies at the pore surface and LAB respectively.

Here, index s stands for subgrain surface.

Introducing boundary conditions (7) and (8) into Eq. (6), we obtain the radial distribution of the concentration of vacancies:

$$c(r) = c_p + (c_s - c_p)\frac{R_s}{R_s - R_p}\left(1 - \frac{R_s}{r}\right) \quad (9)$$

and corresponding concentration gradient

$$\nabla c(r) = \frac{\partial c}{\partial r} = \frac{c_s - c_p}{R_s - R_p}\frac{R_s R_p}{r^2}. \quad (10)$$

The concentration gradient at the pore surface is

$$\nabla c(R_p) = \frac{c_s - c_p}{R_s - R_c}\frac{R_s}{R_p}. \quad (11)$$

According to Fick's first law, the vacancy flow at the pore surface is defined by the following relation:

$$j = -D_V \nabla c(R_p). \quad (12)$$

As follows from Eqs. (11) and (12),

$$j = -D_V \frac{c_s - c_p}{R_s - R_p}\frac{R_s}{R_p}. \quad (13)$$

Equation (13) is the known LeClaire solution for the diffusion flow between two concentric free surfaces with homogeneous distribution of the concentrations of vacancies c_p and c_s, respectively, within each surface. This equation was used in [14] in the analysis of the pore contraction by bulk diffusion of vacancies at the final stage of sintering of the powder material. In this work, a spherical vacuum pore in the center of spherical grain was considered, whose surface (high-angle boundary) is a perfect planar vacancy sink. In the case under consideration, the subgrain surface is LAB, which consists of the network of dislocations with a significant interdislocation distance. A typical misorientation of neighboring dendritic subgrains in superalloy single crystals is ~0.5°. At this misorientation, the interdislocation distance in SAB is nearly 30 nm, that is, ≈80 lattice periods. Therefore, the sink power of this LAB is significantly less than that of a perfect planar sink. This difference can be considered by the introduction of an adjustment factor into Eq. (13), namely, by the relative power of sink of LAB $\eta = k/k_0$, where k is the sink power of LAB and k_0 is the power of perfect planar sink. After this adjustment, c_s in Eq. (13) can be considered equal to c_e, which is defined by Eq. (2):

$$j = -\eta D_V \frac{c_e - c_p}{R_s - R_p}\frac{R_s}{R_p}. \quad (14)$$

The vacancy flow (14) decreases the pore volume at the rate of

$$\frac{dV_p}{dt} = -j4\pi R_p^2. \quad (15)$$

According to [13], the diffusion coefficient of vacancies D_V and the self-diffusion coefficient D are related by following equation:

$$D_V = D/\xi c^0, \quad (16)$$

where ξ is the correlation factor corresponding to 0.781 for FCC crystals.

Introducing Eqs. (14) and (16) into Eq. (15) and assuming that $V_p = 4\pi R_p^3/3$, we get the equation for the rate of decrease in the pore radius:

$$\frac{dR_p}{dt} = \eta\frac{D}{\xi}\frac{c_e - c_p}{c^0}\frac{R_s}{(R_s - R_p)R_p}. \quad (17)$$

After introducing the difference of concentrations $c_e - c_p$ from Eqs. (1) and (2), we have

$$\frac{dR_p}{dt} = \eta\frac{DV_a}{\xi kT}\left(-p - \frac{2\gamma_p}{R_p}\right)\frac{R_s}{(R_s - R_p)R_p}. \quad (18)$$

As was mentioned above, the surface energy is low in nickel and nickel-base superalloys, ~2 J m^{-2} [23–27]; therefore, the second component in square brackets is small for the pores, whose radii are larger than critical, which corresponds to $R_p^* = 2\gamma_p/p$. At the pressures corresponding to industrial HIP of single-crystal blades, $p \sim 100$ MPa the critical pore radius is $R_p^* \sim 2 \times 2$ J m^{-2}/100 MPa = 40 nm. During HIP, the pore slowly contracts under external pressure and, after achieving the critical size, quickly collapses under surface tension. Therefore, in the evaluation of the total time to pore collapse, the latter quick phase and, consequently, the component $2\gamma_p/R_p$ can be neglected. Under this assumption, we get

$$\frac{dR_p}{dt} = -\eta\frac{DV_a}{\xi kT}p\frac{R_s}{(R_s - R_p)R_p}. \quad (19)$$

Because the subgrain radius R_s decreases with a decrease of the pore radius R_p, Eq. (19) should be solved under the condition of conservation of the material volume $d(R_p^3)/dt = d(R_s^3)/dt$. However, because the pore radius is significantly smaller than the subgrain radius (initially by the factor of 7.7) and this ratio grows during HIP, one can assume that $R_p \ll R_s$. This approximation leads to a simple differential equation

$$\frac{dR_p(t)}{dt} = -\eta\frac{DV_a}{\xi kT}pR_p^{-1}, \quad (20)$$

the solution of which is

$$R_p^2(t) = R_p^2(0) - 2\eta\frac{DV_a}{\xi kT}pt. \quad (21)$$

This parabolic dependence of pore contraction during HIP is analogous to known equation for diffusion growth of the pore at a supersaturated concentra-

tion of vacancies [30]; however, it is different in sign and the coefficient before the time t.

A decrease in the volume fraction of pores during HIP $f_p(t)$ can be obtained using the following relation:

$$f_p(t) = f_p(0)\left[\frac{R_p(t)}{R_p(0)}\right]^3. \quad (22)$$

Equation (22) is valid when all pores in the single crystal have the same size. However, in real single crystals, the pore size varies in a broad range, as can be seen in Fig. 7.

The pore size distribution can be considered as follows:

$$f_p(t) = f_p(0)\sum_i \left[\frac{R_{p,i}(t)}{R_{p,i}(0)}\right]^3 q_i, \quad (23)$$

where q_i is the frequency of pores with the radius of $R_{(p,\,i)}(0)$.

To calculate the kinetics of pore annihilation during HIP of CMSX-4 alloy at $T = 1288$°C and pressure $p = 103$ MPa, which is employed by Howmet from the United States, the following parameters were used:

1. Initial volume fraction of pores $f_p(0) = 0.22\%$ [7, 10].

2. Mean equivalent radius of initial pores $R_p(0) = 4.35$ μm (Fig. 7 [2]).

3. Atomic volume V_a at the temperature of HIP was calculated taking into account the thermal expansion of the lattice ε_T. The mean period of the γ/γ′-lattice of CMSX-4 alloy at 20°C $a(20°C) \approx 0.3592$ nm [20]. According to [31], in the case of CMSX-4 alloy, $\varepsilon_T(1288°C) = 0.025$. Using these data, we have $a(1288°C) = a(20°C)[1 + \varepsilon_T(1288°C)] = 0.3592$ nm × (1 + 0.025) = 0.3682 nm and $V_a(1288°C) = a^3/4 = (0.3682 \times 10^{-9}\ \text{m})^3/4 = 1.25 \times 10^{-29}\ \text{m}^3$.

4. Boltzmann constant $k = 1.38 \times 10^{-23}$ J/K.

5. Temperature dependence of the self-diffusion coefficient of nickel $D_{Ni}^{Ni} = \exp(\Delta G/RT)$, $\Delta G = -287000 - 69.8T$ J/mol and $R = 8.314$ J mol^{-1} K^{-1} [32].

6. The correlation factor for FCC crystals $\xi = 0.781$ [13].

There are no data on the sink power of LAB for FCC of nickel alloy with the subgrain size of 30–35 nm at 1288°C. Therefore, to a first approximation, calculated data for FCC of aluminum [18] and copper [19] were used, according to which the normalized sink power η of LAB with misorientation of 0.5° (typical disorientation for dendritic subgrains in single-crystal superalloy) is 0.2–0.3 (Fig. 2). In these calculations, the mean value $\eta = 0.25$ was used.

The results of the calculation are given in Fig. 8. It is seen that the curve of pore annihilation during HIP calculated considering the pore size distribution has the shape similar to the experimental curve, while the curve calculated under the assumption of constant

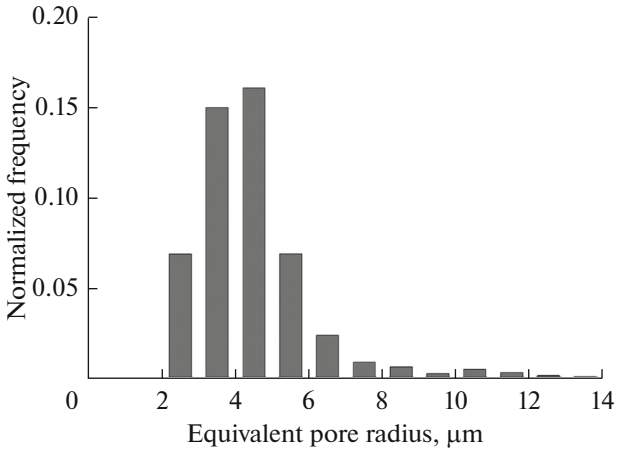

Fig. 7. Histogram of distribution of equivalent pore radius $R_p^{eq} = \sqrt[3]{3V_p/4\pi}$ in heat-treated single crystal of CMSX-4 alloy obtained by processing synchrotron X-ray tomograms [2].

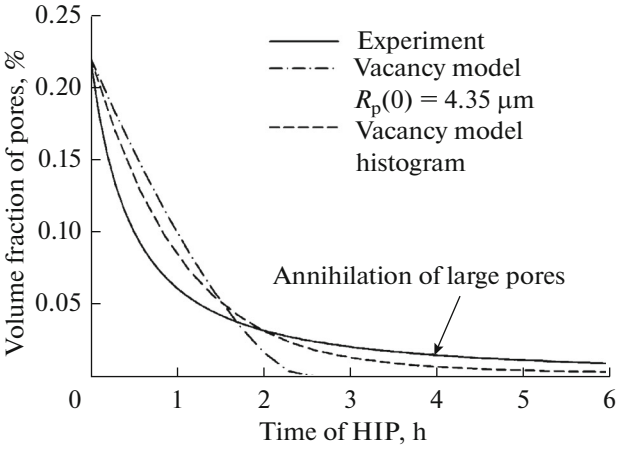

Fig. 8. Kinetics of pore annihilation in heat-treated CMSX-4 alloy during HIP at 1288°C/103 MPa: bold curve stands for experimental results from the measurement of density and qualitative metallography [7, 10], dash-dotted curve is the calculation assuming the equivalent pore size (initial radius is 4.35 μm), and dashed curve is the calculation assuming the pore size distribution.

pore size quickly descends. The reason for a long tail on the first curve is a slow annihilation of large pores. In the material with the given volume fraction of porosity $f_p(0)$, annihilation of the integral porosity occurs more quickly when pores are small and more slowly when pores are large. As follows from Eqs. (14) and (15), the rate of the pore shrinkage $dV_p/dt \sim R_p$; however, the number of pores N in the bulk for the given $f_p(0)$ is inversely proportional to the pore volume, that is, proportional to R_p^{-3}. Therefore, the integral rate of annihilation $(dV_p/dt)N \sim R_p^{-2}$; i.e., it drastically slows down with an increase in the pore size. In

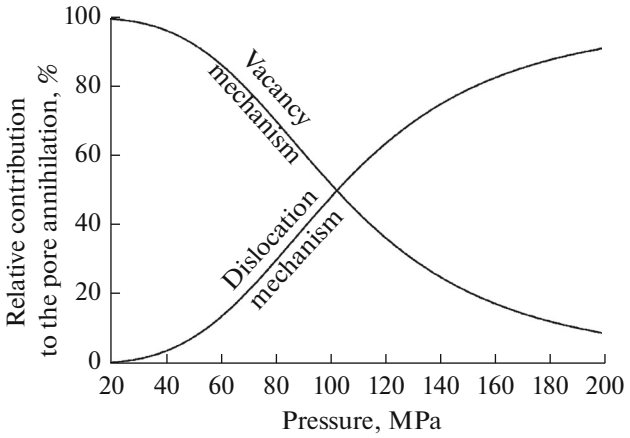

Fig. 9. Change of relative contributions of vacancy and dislocation mechanisms to the pore annihilation during HIP with an increase in pressure. It is hypothesized that the contributions of both mechanisms are equivalent at $p = 103$ MPa.

spite of the visual similarity of calculated and experimental curves, the predicted rate of pore annihilation within 0–2 h is almost two times smaller than the experimental value.

RESULTS AND DISCUSSION

As follows from the results of calculation, pore annihilation during the industrial HIP of single-crystal superalloys can occur by vacancy dissolution of pores and further absorption of vacancies on LAB. The curve of the porosity annihilation in CMSX-4 alloy calculated for HIP at 1288°C/103 MPa is qualitatively similar to the experimental one, but the predicted rate of pore annihilation in the time interval of 0–2 h is almost two times smaller than the experimental value. It should be noted that the rate of the vacancy annihilation of pore is directly proportional to the normalized sink power of LAB η (21), whose exact value for the considered case is unknown.

On the contrary, it was shown in [7, 10] that pore annihilation in CMSX-4 alloy under the same HIP conditions can also occur via the dislocation mechanism. It is evident that the relative contribution of vacancy and dislocation mechanisms changes with stress, because the rate of diffusion mass transfer and Nabarro–Herring diffusion creep is a linear function of stress, while the rate of dislocation creep is an exponential function. For example, in the case of CMSX-4 alloy at 1288°C, the rate of dislocation creep is proportional to stress to the power of $n \approx 4.5$. It is easy to show that the relative contributions of vacancy mechanism X_V and dislocation mechanism X_D to pore annihilation are

$$X_V = \left[1 + (p/p_0)^{n-1}\right]^{-1}, \quad (24)$$

$$X_D = \left[1 + (p_0/p)^{n-1}\right]^{-1}. \quad (25)$$

In Fig. 9, the plots of these dependences are given under the assumption that $X_V = X_D$ at $p_0 = 103$ MPa. It is clear that, with an increase in pressure, the contribution of the dislocation mechanism increases while the contribution of the vacancy mechanism decreases.

In summary, possible further development of the vacancy model could be proposed.

1. It is interesting to consider the model with the location of pore on LAB as occurs in superalloy single crystals (Fig. 1a). It was shown in [14] that the rate of pore annihilation at the grain boundary during sintering of powder materials may exceed many times that for the pore in the grain bulk.

2. From the practical viewpoint, it is interesting to consider the effect of the free surface of single crystal on the rate of pore annihilation, which can be significant during HIP of thin-walled blades with transpiration cooling [33].

3. To increase the reliability of the results, the sink power of LAB in superalloy single crystals should be evaluated quantitatively.

4. The multicomponent diffusion of the alloying elements during HIP should also be considered in order to predict γ' inclusions which are formed upon pore collapse.

CONCLUSIONS

1. An improved model of vacancy dissolution of pores during HIP in the single crystals of nickel-base superalloys considering the absorption of vacancies at low-angle subgrain boundaries was proposed. The model considers the pore size distribution and predicts the kinetics of pore annihilation similar to the experimental one. It was shown that the presence of large pores slows down the annihilation process, and this fact should be taken into account in the choice of the duration of industrial HIP.

2. To identify the mechanism of pore annihilation during HIP, the exponent of function $dV_p/dt \sim \sigma^n$ should be determined. At $n \approx 1$, the mechanism of pore annihilation is vacancy, whereas at n significantly larger than 1 it is dislocation. In addition, a detailed TEM study of local dislocation mechanisms and concentration microgradients at the surface of partially shrank pores after HIP of limited duration should also be carried out.

ACKNOWLEDGMENTS

This work was supported by the German Research Foundation DFG (projects EP 136/1-1 and FE933/2-1) and the French National Research Agency ANR (projects ANR15-MERA-000-03 and ANR15-MERA-0003-04).

REFERENCES

1. Epishin, A., Link, T., Bruckner, U., and Portella, P.D., Investigation of porosity in single-crystal nickel-base superalloys, *Proc. 7th Liege Conf. on Materials for Advanced Power Engineering,* Jülich: Forschungszentrum Jülich, 2002, pp. 217–226.
2. Link, T., Zabler, S., Epishin, A., Haibel, A., Bansal, M., and Thibault, X., Synchrotron X-ray tomography of porosity in single-crystal nickel base superalloys, *Mat. Sci. Eng., A,* 2006, vol. 425, pp. 47–54.
3. Epishin, A., Link, T., Svetlov, I.L., Nolze, G., Neumann, R.S., and Lucas, H., Mechanism of porosity growth during homogenisation in single crystal nickel-based superalloys, *Int. J. Mater. Res.*, 2013, vol. 104, pp. 776–782.
4. Lecomte-Beckers, J., Study of microporosity formation in nickel-base superalloys, *Metall. Trans. A,* 1988, vol. 19, no. 9, pp. 2341–2348.
5. Anton, D.L. and Giamei, A.F., Porosity distribution and growth during homogenization in single crystals of a nickel-base superalloy, *Mater. Sci. Eng.,* 1985, vol. 76, pp. 173–180.
6. Toloraya, V.N., Zuev, A.G., and Svetlov, I.L., Effect of conditions of directed solidification and heat treatment on porosity in creep resistant nickel alloy single crystals, *Izv. Akad. Nauk SSSR, Met.,* 1991, no. 5, pp. 70–76.
7. Epishin, A.I., Link, T., Fedelich, B., Svetlov, I.L., and Golubovskiy, E.R., Hot isostatic pressing of single-crystal Ni-based superalloys: mechanism of pore closure and effect on mechanical properties, *Proc. 2nd Eur. Symp. on Superalloys and their Applications (EUROSUPERALLOYS 2014),* Les Ulis: EDP Sciences, 2014, vol. 14. 08003.
8. Bokstein, B., Epishin, A., Esin, V., Mendelev, M., Rodin, A., and Zhevnenko, S., Cross diffusion-stress effects, *Defect Diffus. Forum,* 2007, vol. 264, pp. 79–89.
9. Bokstein, B.S., Epishin, A.I., Esin, V.A., Rodin, A.O., Svetlov, I.L., and Link, T., Growth and healing of porosity in single-crystals of nickel-base superalloys, *J. Funct. Mater.,* 2007, vol. 1, no. 5, pp. 162–169.
10. Epishin, A., Fedelich, B., Link, T., Feldmann, T., and Svetlov, I.L., Pore annihilation in a single-crystal nickel-base superalloy during hot isostatic pressing: Experiment and modelling, *Mater. Sci. Eng., A,* 2013, vol. 586, pp. 342–349.
11. Mujica Roncery, L., Lopez-Galilea, I., Ruttert, B., Huth, S., and Theisen, W., Influence of temperature, pressure, and cooling rate during hot isostatic pressing on the microstructure of an SX Ni-based superalloy, *Mater. Des.,* 2016, vol. 97, pp. 544–552.
12. Coble, R.L., Sintering crystalline solids: I. Intermediate and final state diffusion models, *J. Appl. Phys.,* 1961, vol. 32, no. 5, pp. 787–792.
13. Volin, T.E. and Balluffi, R.W., Annealing kinetics of voids and the self-diffusion coefficient in aluminium, *Phys. Stat. Sol.,* 1968, vol. 25, pp. 163–173.
14. Rosolowski, J.H. and Greskovich, C., Analysis of pore shrinkage by volume diffusion during final stage of sintering, *J. Appl. Phys.,* 1973, vol. 44, no. 4, pp. 1441–1450.
15. Park, J.-W. and Altstetter, C.J., The diffusion and solubility of oxygen in solid nickel, *Metall. Trans. A,* 1987, vol. 18, pp. 43–50.
16. Kowanda, C. and Speidel, M.O., Solubility of nitrogen in liquid and binary Ni—X_i alloys (X_i = Cr, Mo, W, Mn, Fe, Co) under elevated pressure, *Scr. Mater.,* 2003, vol. 48, pp. 1073–1078.
17. Balluffi, R.W., Grain boundary diffusion mechanisms in metals, *Metall. Trans. A,* 1982, vol. 13, pp. 2069–2095.
18. King, A.H. and Smith, D.A., Calculation of sink strength and bias for point-defect absorption by dislocations in arrays, *Radiat. Eff.,* 1981, vol. 54, pp. 169–176.
19. Jiang, C., Swaminathan, N., Deng, J., Morgan, D., and Szlufarska, I., Effect of grain boundary stresses on sink strength, *Mater. Res. Lett.,* 2014, vol. 2, no. 2, pp. 100–106.
20. Bruckner, U., Epishin, A., and Link, T., Local x-ray diffraction analysis of the structure of dendrites in single-crystal nickel-base superalloys, *Acta Mater.,* 1997, vol. 45, no. 2, pp. 5223–5231.
21. Bruckner, U., Epishin, A., Link, T., and Dressel, K., The influence of the dendritic structure on the γ/γ′—lattice misfit in the single-crystal nickel-base superalloy CMSX-4, *Mater. Sci. Eng., A,* 1998, vol. 247, pp. 23–31.
22. Epishin, A.I., Rodin, A.O., Bokstein, B.S., Oder, G., Link, T., and Svetlov, I.L., Interdiffusion in binary Ni–Re alloys, *Phys. Met. Metallogr.,* 2015, vol. 116, pp. 175–181.
23. Epishin, A.I. and Svetlov, I.L., Evolution of pore morphology in single-crystals of nickel-base superalloys, *Inorg. Mater.: Appl. Res.,* 2016, vol. 7, no. 1, pp. 45–52.
24. Tyson, W.R. and Miller, W.A., Surface free energies of solid metals estimation from liquid surface tension measurements, *Surf. Sci.,* 1977, vol. 62, pp. 267–276.
25. Vitos, L., Ruban, A.V., Skriver, H.L., and Kollár, J., The surface energy of metals, *Surf. Sci.,* 1998, vol. 411, pp. 186–202.
26. Brillo, J. and Egry, I., Surface tension of nickel, copper, iron and their binary alloys, *J. Mater. Sci.*, 2005, vol. 40, pp. 2213–2216.
27. Aqra, F. and Ayyad, A., Surface energies of metals in both liquid and solid states, *Appl. Surf. Sci.,* 2011, vol. 257, pp. 6372–6379.
28. Giuranno, D., Amore, S., Novakovich, R., and Ricci, E., Surface tension and density of RENE N5 and RENE 90 Ni-base superalloys, *J. Mater. Sci.,* 2015, vol. 50, pp. 3763–3771.
29. Wang, H. and Li, Z., Diffusive shrinkage of a void within a grain of a stressed polycrystal, *J. Mech. Phys. Solids,* 2003, vol. 51, pp. 961–976.
30. Cuitiño, A.M. and Ortiz, M., Ductile fracture by vacancy condensation in f. c. c. single crystals, *Acta Mater.,* 1996, vol. 44, pp. 427–436.
31. Epishin, A., Link, T., Brückner, U., and Fedelich, B., Residual stresses in the dendritic structure of single crystal nickel-based superalloys, *Phys. Met. Metallogr.,* 2005, vol. 100, no. 2, pp. 104–112.
32. Engström, A. and Ågren, J., Assessment of diffusional mobilities in face-centered cubic Ni–Cr–Al alloys, *Z. Metallkd.,* 1996, vol. 87, pp. 92–97.
33. Liang, G., US Patent 6808367, 2004.

Translated by A. Muravev